Photoproduction of jets at DESY HERA in next-to-leading order QCD

B. W. Harris and J. F. Owens

Physics Department, Florida State University, Tallahassee, Florida 32306-4350

A new next-to-leading order Monte Carlo program for the calculation of jet cross sections in photoproduction is described. The contributions from both resolved and direct components are included to $O(\alpha\alpha_s^2)$. Properties of the predictions for various inclusive jet and dijet observables are discussed and comparisons with DESY HERA data are presented. [S0556-2821(97)01719-0]

I. INTRODUCTION

Electromagnetic interactions have long been used to study both hadronic structure and strong interaction dynamics. Examples include deep inelastic lepton-nucleon scattering, hadronic production of lepton pairs, the production of photons with large transverse momenta, and various photoproduction processes involving the scattering of real or very low mass virtual photons from hadrons. In particular, the photoproduction of jets with large transverse momenta is calculable in QCD and offers additional complementary information to that obtained from the study of the hadroproduction of jets [1]. In the photoproduction case there are contributions where the photon's energy contributes entirely to the hard-scattering subprocess; these are often referred to collectively as the direct component. In addition, a real photon can interact via its hadronic substructure. These contributions comprise the resolved component, a review of which is contained in Ref. [2]. Therefore, the photoproduction of jets allows one to investigate new production mechanisms, probe the hadronic substructure of the photon, and study the conventional hadronic jet production mechanisms which these processes have in common with the hadroproduction case.

Two basic approaches are commonly employed for generating predictions for hard-scattering processes. On the one hand, it is possible to perform calculations for a specific observable in which the integrals over the subprocess variables are done analytically, leaving only the convolutions with the parton distributions to be done numerically. On the other hand, if the subprocess integrations and the parton distribution convolutions are done using Monte Carlo techniques, it is possible to generate predictions for a variety of different observables simultaneously. This latter approach is sometimes referred to as a fully differential Monte Carlo calculation. Several groups have performed next-to-leading order calculations of jet photoproduction in varying degrees of generality using one or the other of these two approaches. In [3–5] subprocesses which involved the photon were kept up to $O(\alpha\alpha_s^2)$. Thus, the direct component was calculated to next-to-leading-logarithm accuracy while the resolved component was calculated in the leading-logarithm approximation. The resolved component was calculated to next-to-leading-logarithm accuracy in [6–9] for single inclusive production. For a review see [10]. Recently, both direct and resolved contributions calculated to next-to-leading-logarithm accuracy have begun to appear [11–13] in a fully differential form.

The purpose of this work is to present a discussion of a calculation which is based on the phase space slicing method using two cutoffs [14]. Both the direct and resolved components are included to next-to-leading-logarithm accuracy. The result is fully differential and implemented in a Monte Carlo style program which allows the simultaneous histogramming of many distributions incorporating experimental cuts. It represents an improvement of earlier results which included the direct component only at next-to-leading order (NLO) [3] and an elaboration of the very brief results for both components already presented [11]. Details of the calculational method are presented as well as comparisons with recent data. Some comments on various unsettled issues that arise when comparing with dijet cross sections are also given.

The remainder of the paper is as follows. The phase space slicing method is reviewed in Sec. II. Numerical results are compared with H1 and ZEUS data and related physics issues are discussed in Sec. III, while the conclusions are given in Sec. IV.

II. METHOD

In this section we describe the calculation of QCD corrections to two-jet production in electron-proton scattering using the phase space slicing method. Before discussing the QCD corrections, it is necessary to recount the connection between electron-proton and photon-proton scattering. For small photon virtualities Q^2 the two are related using the Weizsäcker-Williams approximation [15] wherein one assumes that the incoming electron beam is equivalent to a broadband photon beam. The cross section for electron-proton scattering is then given as a convolution of the photon distribution in an electron and the photon-proton cross section

$$d\sigma(ep \to eX) = \int_{y_{\min}}^{y_{\max}} dy \, F_{\gamma/e}(y) d\sigma(\gamma p \to X). \quad (2.1)$$

The integration limits and the maximum photon virtuality $Q_{\max}^2$ are determined from the (anti)tagging conditions of the experiment. The energy of the photon is related to the energy of the incident electron by $E_\gamma = yE_e$. We used the improved photon distribution in an electron [16] given by the formula

$$F_{\gamma/e}(y) = \frac{\alpha_{\rm em}}{2\pi}\left\{\frac{1+(1-y)^2}{y}\ln\frac{Q_{\rm max}^2(1-y)}{m_e^2 y^2}\right.$$
$$\left.+2m_e^2 y\left[\frac{1}{Q_{\rm max}^2}-\frac{1-y}{m_e^2 y^2}\right]\right\}, \qquad (2.2)$$

where m_e is the electron mass and $\alpha_{\rm em}$ is the electromagnetic coupling. Within this approximation, QCD corrections to electron-proton scattering correspond to QCD corrections to photon-proton scattering to which we now turn.

In this version of the phase space slicing method [14] two small cutoffs δ_s and δ_c are used to delineate regions of phase space where soft and collinear singularities occur. Let the four vectors of the three-body subprocesses be labeled $p_1 + p_2 \to p_3 + p_4 + p_5$, and define the Mandelstam invariants $s_{ij} = (p_i + p_j)^2$ and $t_{ij} = (p_i - p_j)^2$. Consider, for example, the $\gamma(p_1)g(p_2) \to q(p_3)\bar{q}(p_4)g(p_5)$ subprocess whose matrix element becomes singular as the energy E_5 of the final state gluon becomes soft. Define the soft region S by $0 < E_5 < \delta_s\sqrt{s_{12}}/2$ and the complementary hard region H by $\delta_s\sqrt{s_{12}}/2 < E_5 < \sqrt{s_{12}}/2$, both in the $p_1 + p_2$ rest frame. The two-to-three-body contribution to the cross section is then decomposed as

$$\sigma = \frac{1}{2s_{12}}\int |M|^2 d\Gamma_3 = \frac{1}{2s_{12}}\int_S |M|^2 d\Gamma_3$$
$$+\frac{1}{2s_{12}}\int_H |M|^2 d\Gamma_3, \qquad (2.3)$$

where $|M|^2$ is the three-body squared matrix element and $d\Gamma_3$ is the three-body phase space. Within S one sets $p_5 = 0$ *everywhere* except in the denominators of the matrix elements and then analytically integrates over the unobserved degrees of freedom in n space-time dimensions. The result, proportional to the leading order cross section, contains double and single poles in $n-4$, and double and single logarithms in the soft cutoff δ_s. Terms of order δ_s are neglected. Next, the collinear regions of phase space are defined to be those where any invariant (s_{ij} or t_{ij}) becomes smaller in magnitude than $\delta_c s_{12}$. The hard region is then decomposed into collinear C, and noncollinear $\bar{C}$, regions as follows:

$$\frac{1}{2s_{12}}\int_H |M|^2 d\Gamma_3 = \frac{1}{2s_{12}}\int_{HC} |M|^2 d\Gamma_3$$
$$+\frac{1}{2s_{12}}\int_{H\bar{C}} |M|^2 d\Gamma_3. \qquad (2.4)$$

Within HC one retains only the leading pole of the vanishing invariant in the squared matrix elements. Exact collinear kinematics are used to define the integration domain of HC, which is valid so long as $\delta_c \ll \delta_s$. The integrations over the unobserved degrees of freedom are then performed analytically in n space-time dimensions giving a factorized result where single poles in $n-4$, and single logarithms in both cutoffs δ_c and δ_s, multiply splitting functions and lower-order squared matrix elements. Terms of order δ_c and δ_s are neglected. The soft and final state hard collinear singularities cancel upon addition of the interference of the leading order diagrams with the renormalized one-loop virtual diagrams.

The remaining initial state collinear singularities are factorized and absorbed into the parton distributions. The integrations over the singularity-free portion of the three-body phase space $H\bar{C}$ are performed using standard Monte Carlo techniques. When all of the contributions are combined at the histogramming stage the cutoff dependences cancel, provided one looks at a suitably defined infrared-safe observable. An example will be given below.

The matrix elements squared for all two-to-two and two-to-three parton-parton scattering subprocesses through $O(\alpha_s^3)$ are from the paper of Ellis and Sexton [17], and those for the photon-parton scattering subprocesses through $O(\alpha \alpha_s^2)$ are from the paper of Aurenche *et al.* [18].

In order to compare with experimental data, a suitable jet definition must be chosen. For this study, the algorithm of Huth *et al.* [19] has been used, supplemented with an $R_{\rm sep}$ constraint [20] as follows. Let η_i (η_j) be the pseudorapidity and ϕ_i (ϕ_j) be the azimuthal angle of parton i (j) and then define

$$R_{ij} = [(\eta_i - \eta_j)^2 + (\phi_i - \phi_j)^2]^{1/2}. \qquad (2.5)$$

Partons i and j are merged if

$$R_{ij} \leq \min\left[\frac{E_{T_i}+E_{T_j}}{\max(E_{T_i},E_{T_j})}R, R_{\rm sep}\right]. \qquad (2.6)$$

Note that $R_{\rm sep} = 2R$ corresponds to having no $R_{\rm sep}$ constraint. The four-vector recombination is of the type

$$E_T^{\rm jet} = E_T^i + E_T^j,$$
$$\eta^{\rm jet} = (\eta^i E_T^i + \eta^j E_T^j)/E_T^{\rm jet},$$
$$\phi^{\rm jet} = (\phi^i E_T^i + \phi^j E_T^j)/E_T^{\rm jet}. \qquad (2.7)$$

Other types of jet algorithms may also be used.

III. RESULTS

A. General properties

Using the results of the method described in the previous section we have constructed a program to calculate jet photoproduction cross sections. The program uses Monte Carlo integration so it is possible to implement experimental cuts, provided that they are defined in terms of partonic variables.

The CTEQ4 [21] proton parton distribution set was used throughout, in conjunction with either the Glück-Reya-Vogt (GRV) [22] or Gordon-Storrow (GS) [23] photon set. Unless otherwise noted, the GRV set was used. The calculation was performed in the modified minimal subtraction ($\overline{\rm MS}$) factorization scheme. Therefore, the corresponding $\overline{\rm MS}$ distribution sets were used when working at next-to-leading order (NLO). For leading order (LO) results, the appropriate LO sets were used. Similarly, the two-loop version of the strong coupling α_s was used with matching across quark thresholds for the NLO results, and at LO the one-loop value was used. The value of $\Lambda^{\rm QCD}$ was taken from the proton parton distribution set.

For future use we define three sets of beam energy and tagging conditions as follows: 1993 H1 where $E_e = 26.7$
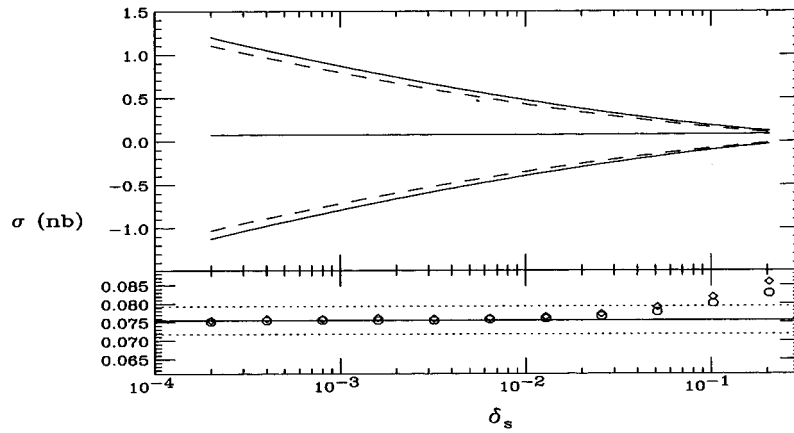
FIG. 1. The single-jet inclusive cross section integrated over 30 GeV$<E_T^{\text{jet}}<$40 GeV and $0<\eta^{\text{jet}}<2$. The two-body (negative) and three-body (positive) contributions together with their sum are shown as a function of δ_s with $\delta_c=\delta_s/a$ for $a=100$ (dash line) and $a=200$ (solid line). The bottom enlargement shows the sum for $a=100$ (circles) and $a=200$ (diamonds) relative to $\pm5\%$ (dotted line) of the average of the last four points (solid line).

GeV, $E_p=820$ GeV, $Q_{\text{max}}^2=0.01$ GeV^2, and $0.25<y<0.7$, 1993 ZEUS where $E_e=26.7$ GeV, $E_p=820$ GeV, $Q_{\text{max}}^2=4$ GeV^2, and $0.2<y<0.85$, and finally 1994 ZEUS where $E_e=27.5$ GeV, $E_p=820$ GeV, $Q_{\text{max}}^2=4$ GeV^2, and $0.25<y<0.8$.

As explained above, when contributions from the two-body and three-body pieces are combined to form a suitably defined infrared-safe observable the cutoff dependences cancel. This provides a check on the method and also on its implementation. As stated in Sec. II, the method requires that $\delta_c\ll\delta_s$. Therefore, we take $\delta_c=\delta_s/a$ with $a\sim100$ and verify that the result is independent of a. As an example, the single-jet inclusive cross section integrated over 30 GeV $<E_T^{\text{jet}}<40$ GeV and $0<\eta^{\text{jet}}<2$ is shown in Fig. 1 for the 1994 ZEUS conditions with $R=1$ and $R_{\text{sep}}=2$. The two-body (negative) and three-body (positive) contributions together with their sum are shown as a function of δ_s for $a=100$ (dashed line) and $a=200$ (solid line). The bottom enlargement shows the sum for $a=100$ (circles) and $a=200$

(diamonds) relative to $\pm5\%$ (dotted line) of the actual result (solid line). For this particular observable, the result is sufficiently independent of the cutoffs below $\delta_s=10^{-2}$.

One of the primary reasons for carrying out a NLO calculation is that of reducing factorization and renormalization scale dependence. This is illustrated in Fig. 2 for the single-jet inclusive cross section as a function of E_T^{jet} integrated over $-1<\eta^{\text{jet}}<2$ for the 1993 H1 conditions with $R=1$ and $R_{\text{sep}}=2$. The factorization and renormalization scales have been set equal to μ. The LO (dash line) and NLO (solid line) results are shown for two different scale choices $\mu=E_T^{\text{max}}/2$ (top) and $\mu=2E_T^{\text{max}}$ (bottom) where E_T^{max} is the maximum transverse energy associated with the relevent two- or three-body weight. The single-jet inclusive cross section as a function of η^{jet} integrated over $E_T^{\text{jet}}>15$ GeV is shown in Fig. 3. In both cases, the NLO calculation shows reduced scale dependence relative to the LO result.

As stated in the Introduction, it is conventional to describe jet photoproduction in terms of two components. The direct
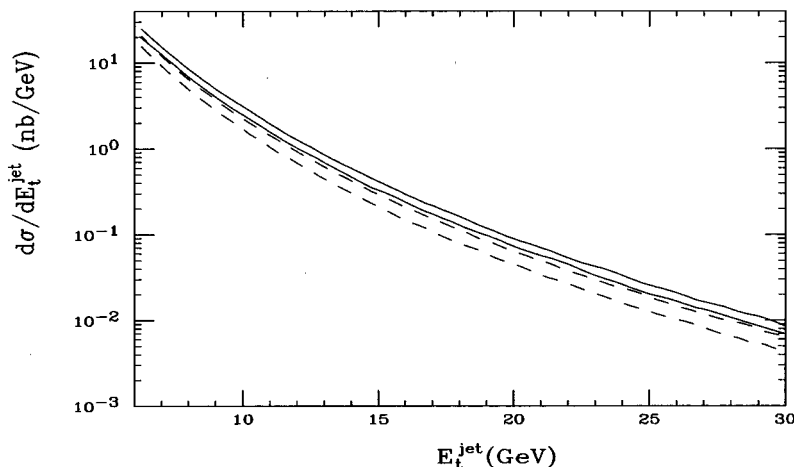

FIG. 2. Scale dependence of the single-jet inclusive cross section as a function of E_T^{jet} integrated over $-1<\eta^{\text{jet}}<2$. The LO (dash line) and NLO (solid line) results are shown for two different scale choices, $\mu=E_T^{\text{max}}/2$ (top) and $\mu=2E_T^{\text{max}}$ (bottom).
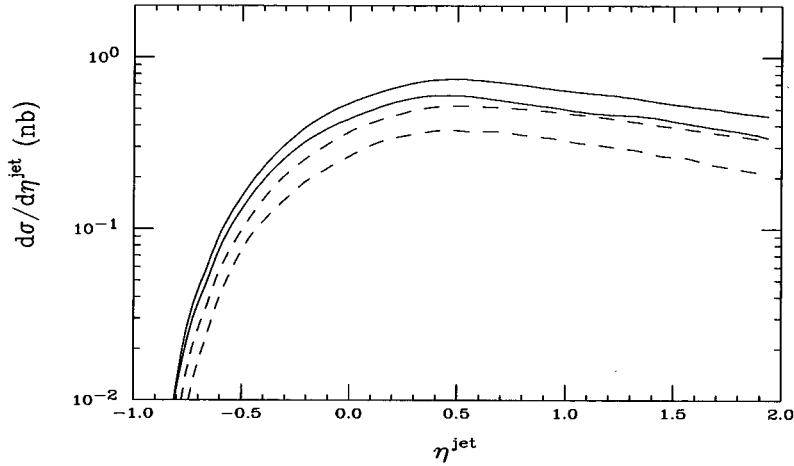
FIG. 3. Scale dependence of the single-jet inclusive cross section as a function of $\eta^{\rm jet}$ integrated over $E_T^{\rm jet} > 15$ GeV. The LO (dash line) and NLO (solid line) results are shown for two different scale choices $\mu = E_T^{\rm max}/2$ (top) and $\mu = 2E_T^{\rm max}$ (bottom).

or pointlike component corresponds to the case where the photon participates wholly in the hard-scattering subprocess, whereas the resolved or hadronlike component corresponds to a situation where the photon interacts as if it contained partons. In the direct component there is, then, no remnant beam jet and this leads to a simpler event structure than in the purely hadronic case. The decomposition is, however, an artifact of viewing the process from the perspective of leading order QCD. At next-to-leading order, the two components mix and a complete separation is not possible.

Although a strict separation into direct and resolved components is not possible, one can still define kinematic regions where either component dominates. One such definition [24] uses the *observed* momentum fraction x_γ of the parton coming from the photon which is given by

$$x_\gamma = (E_T^{\rm jet1} e^{-\eta_{\rm jet_1}} + E_T^{\rm jet2} e^{-\eta_{\rm jet_2}})/2E_\gamma. \qquad (3.1)$$

Here E_T and η are those of the two highest transverse energy jets. The region $x_\gamma > 0.75$ corresponds primarily to the direct contribution and $x_\gamma < 0.75$ to the resolved contribution.

It is interesting to see how the two components populate phase space. To this end, shown in Fig. 4 is the NLO single jet inclusive cross section as a function of $E_T^{\rm jet}$ integrated over $-1 < \eta^{\rm jet} < 2$ in three different regions $0 < x_\gamma < 1$ (solid), $x_\gamma > 0.75$ (dotted), and $x_\gamma < 0.75$ (dashed) for the 1993 ZEUS conditions with $R = 1$, and $R_{\rm sep} = 2$. The cross section dominated by the resolved component has a steeper E_T dependence than that which is dominated by the direct component. This is due to the extra convolution associated with the photon parton distribution. In other words, only a portion of the photon's energy contributes to the hard scattering for the resolved component. Hence, at large E_T values the direct component dominates. In Fig. 5 the NLO single-jet inclusive cross section is shown as a function of $\eta^{\rm jet}$ integrated over $E_T^{\rm jet} > 17$ GeV. The direct component dominates at negative rapidity whereas the resolved component takes over in the positive direction. In the coordinate system used in the experiments at the DESY ep collider HERA, positive rapidity corresponds to the direction of the proton beam. Therefore, if the observed jet is in the positive rapidity re-
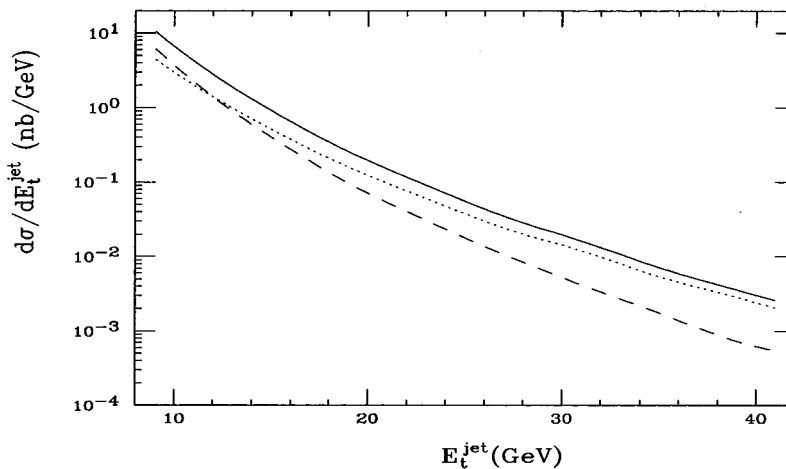

FIG. 4. The NLO single-jet inclusive cross section as a function of $E_T^{\rm jet}$ integrated over $-1 < \eta^{\rm jet} < 2$ in three different regions $0 < x_\gamma < 1$ (solid), $x_\gamma > 0.75$ (dotted), and $x_\gamma < 0.75$ (dashed).
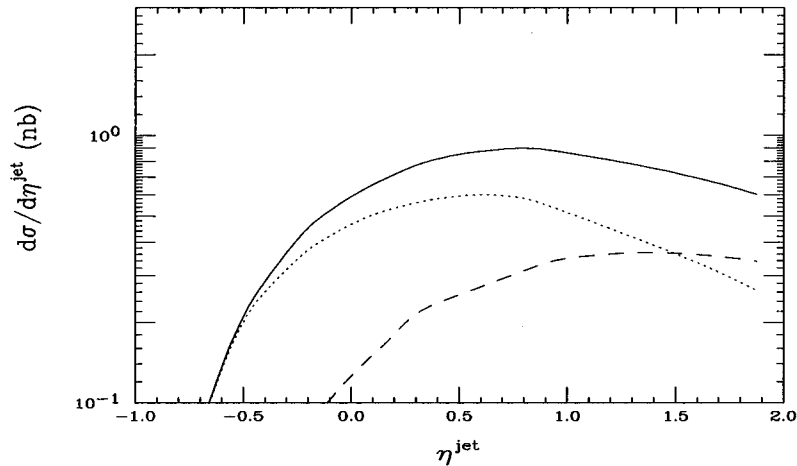
FIG. 5. The NLO single-jet inclusive cross section as a function of η^{jet} integrated over $E_T^{\mathrm{jet}}>17$ in three different regions $0<x_\gamma<1$ (solid), $x_\gamma>0.75$ (dotted), and $x_\gamma<0.75$ (dashed).

gion, this corresponds to larger x values from the proton and smaller ones from the photon. Conversely, if the jet is in the negative rapidity region, larger photon x values and smaller proton x values are favored. Since the contribution dominated by the direct component has $x_\gamma>0.75$, it dominates in the negative rapidity region, as shown. In Fig. 6 the dijet cross section is shown as a function of the invariant mass of the two highest E_T jets. Again, the steeper resolved component dominates over the flatter direct component at low M_{JJ}.

B. Comparison to single inclusive data

Having discussed the general properties of the predictions, it is of interest to see how they compare with existing data. The first comparison is to the single-jet inclusive cross sections as measured by H1 [25]. The single-jet inclusive cross section as a function of E_T^{jet} along with our NLO result (GS photon, solid lines; GRV photon, dashed lines) for the 1993 H1 conditions with $\mu=E_T^{\mathrm{max}}$, $R=1$, and $R_{\mathrm{sep}}=2$ is shown in Fig. 7. The data and theory have different slopes with the theory falling below the data at low E_T^{jet} for both

photon sets. The agreement is slightly better for the case where $\eta^{\mathrm{jet}}<1$. This is seen more clearly in Fig. 8 which shows the single-jet inclusive cross section as a function of η^{jet} for $E_T^{\mathrm{jet}}>E_T^{\mathrm{min}}$ with $E_T^{\mathrm{min}}=7$, 11, and 15 GeV. In the proton direction the theory consistently undershoots the data. The agreement improves as E_T^{min} increases. One possible explanation for the observed discrepency may be the need to increase the gluonic content of the photon which is poorly constrained in this x region. However, it should be noted that underlying event contributions, which were not removed from the data set or included in our calculation, may also provide an explanation.

We next switch to 1993 ZEUS conditions and compare to the published ZEUS data [26] on single-jet inclusive cross sections. In Fig. 9 the measured single-jet inclusive cross section is shown as a function of E_T^{jet} along with our NLO result (GS photon, solid lines; GRV photon, dashed lines) with $\mu=E_T^{\mathrm{max}}$, $R=1$, and $R_{\mathrm{sep}}=2$. In this case the agreement with the data is somewhat better than that shown in Fig. 7. This is further illustrated by the comparison with the single-jet inclusive cross section as a function of η^{jet}, shown in Fig.
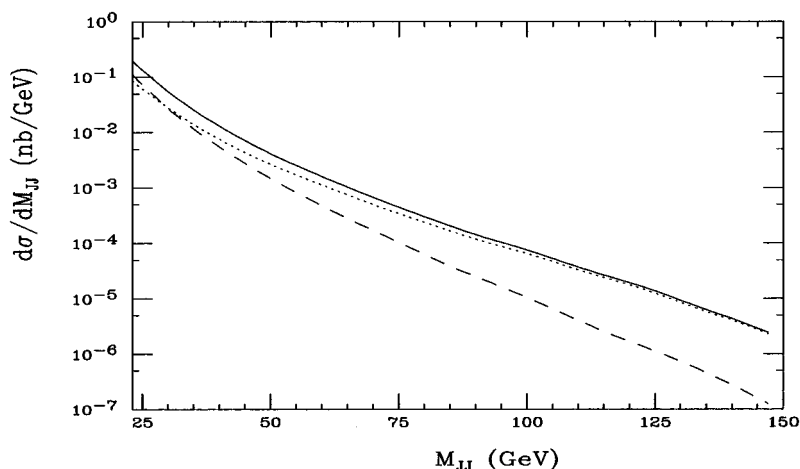

FIG. 6. Dijet cross section as a function of the invariant mass of the two highest E_T jets decomposed into the regions $0<x_\gamma<1$ (solid), $x_\gamma>0.75$ (dotted), and $x_\gamma<0.75$ (dashed).
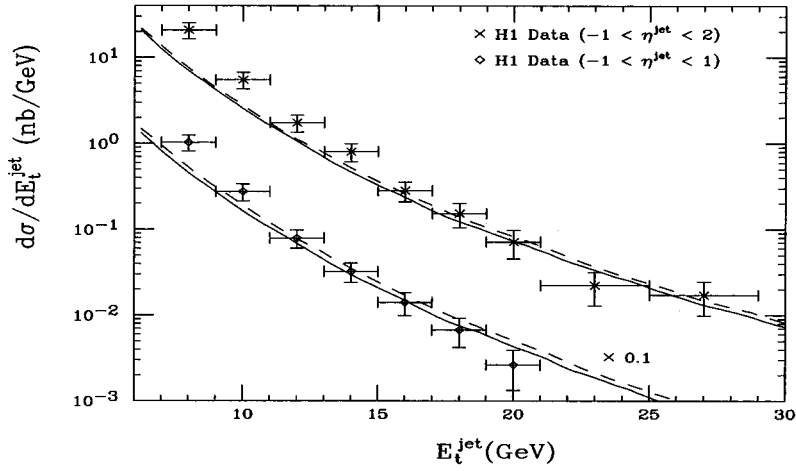
FIG. 7. The single-jet inclusive cross section as a function of E_T^{jet} as measured by H1 [25] compared with our NLO result (GS photon, solid lines; GRV photon, dashed lines).
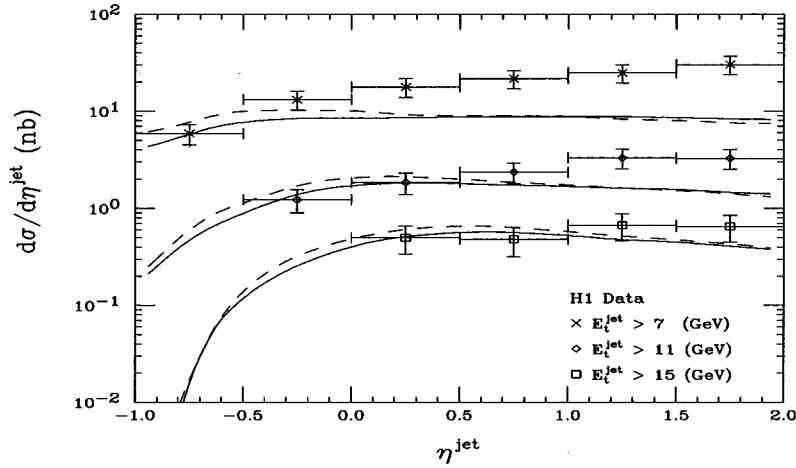

FIG. 8. The single-jet inclusive cross section as a function of η^{jet} as measured by H1 [25] compared with our NLO result (GS photon, solid lines; GRV photon, dashed lines).
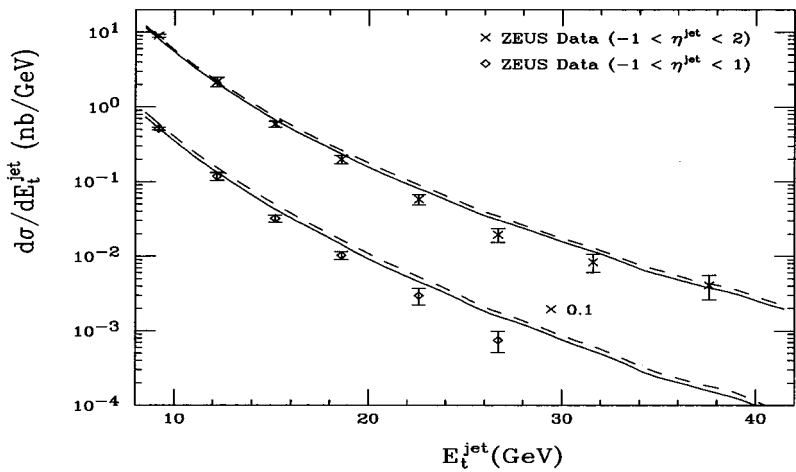

FIG. 9. The single-jet inclusive cross section as a function of E_T^{jet} as measured by ZEUS [26] compared with our NLO result (GS photon, solid lines; GRV photon, dashed lines).
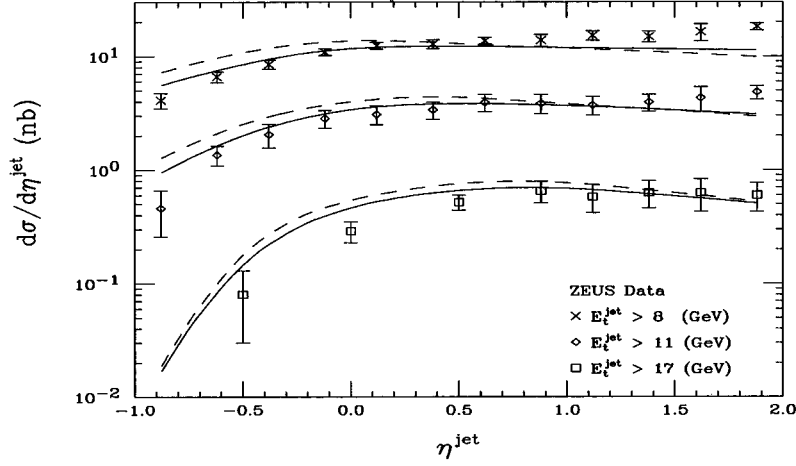
FIG. 10. The single-jet inclusive cross section as a function of η^{jet} as measured by ZEUS [26] compared with our NLO result (GS photon, solid lines; GRV photon, dashed lines).

10. The trend, although less pronounced, is the same as with the H1 data.

C. Comparison to dijet data

Data for several different types of observables involving two large transverse momentum jets have been published. In the ZEUS dijet analysis a sample of dijet events is obtained by requiring $E_T^{\mathrm{jet}_1}, E_T^{\mathrm{jet}_2} > E_T^{\mathrm{min}}$. In principle, this presents a problem in the following sense. The pair of jets can be accompanied by additional soft gluons. The singularities associated with the soft gluon emission cancel infrared singularities coming from one-loop contributions. This cancellation has already taken place in the present calculation. That is, the soft gluons with energies up to $\delta_s \sqrt{s_{12}}/2$ have already been integrated out. After the cancellation there are residual $\ln \delta_s$ terms in the two-body portion of the calculation which can-

cel against logarithms built up by integrating over the unobserved gluon radiation in the three body contribution. The requirement that both jets have $E_T > E_T^{\mathrm{min}}$ restricts a portion of this integration and leads to an incomplete cancellation of the $\ln \delta_s$ dependence. We have, nevertheless, used this definition for the dijet sample, having found that the cutoff dependence of the results is negligible. However, the problem still exists, at least in principle.

Preliminary ZEUS data [27] for the dijet cross section as a function of $\overline{\eta} = (\eta^{\mathrm{jet}_1} + \eta^{\mathrm{jet}_2})/2$ integrated over $|\eta^{\mathrm{jet}_1} - \eta^{\mathrm{jet}_2}| < 0.5$ are shown in Figs. 11 and 12 for $E_T^{\mathrm{jet}_1}, E_T^{\mathrm{jet}_2} > E_T^{\mathrm{min}}$ with $E_T^{\mathrm{min}} = 6, 8, 11$, and 15 GeV. The solid curves are our results for the 1994 ZEUS conditions with $0.2 < y < 0.8$ using the GRV photon set, $\mu = E_T^{\mathrm{max}}/2$, and $R = 1$. A value of $R_{\mathrm{sep}} = 1$ was used following [28] where it was found that this value used at the parton level most closely corresponds to the
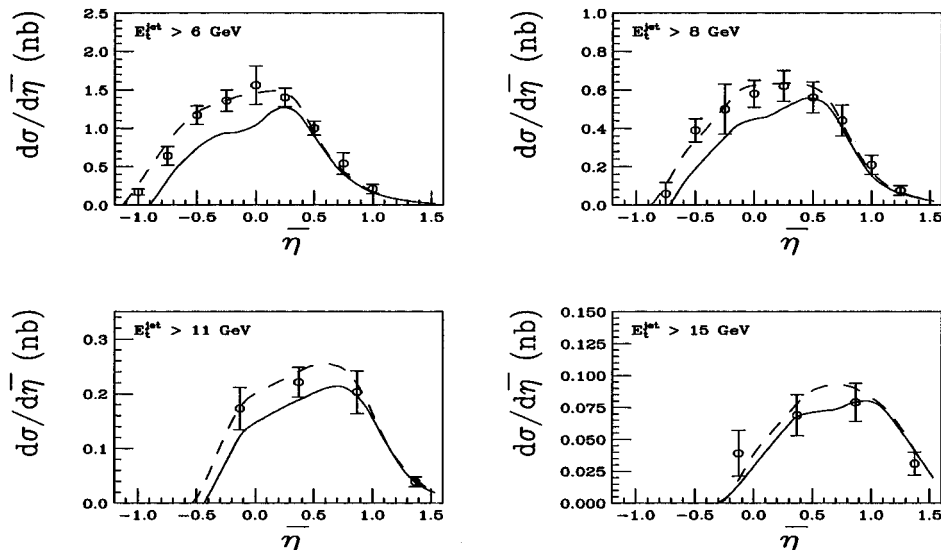

FIG. 11. Dijet cross section for $x_\gamma > 0.75$ as a function of $\overline{\eta}$ integrated over $E_T^{\mathrm{jet}} > E_T^{\mathrm{min}}$ for $E_T^{\mathrm{min}} = 6, 8, 11, 15$ GeV as measured by ZEUS [27]. The solid curves correspond to requiring $E_T^{\mathrm{jet}_1}, E_T^{\mathrm{jet}_2} > E_T^{\mathrm{min}}$ while the dashed curves correspond to the cuts used in [12], as described in text.

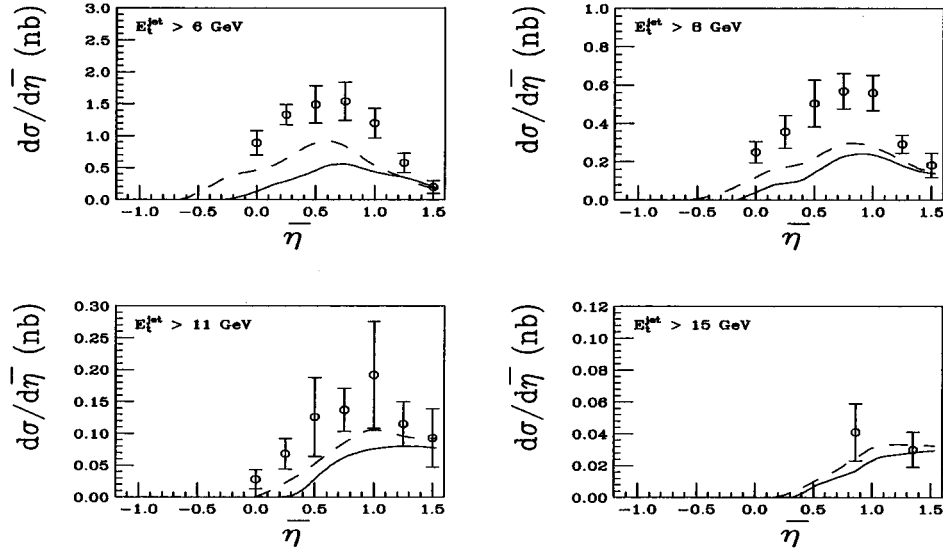FIG. 12. Dijet cross section for $0.3 < x_\gamma < 0.75$ as a function of $\bar\eta$ integrated over $E_T^{\mathrm{jet}} > E_T^{\mathrm{min}}$ for $E_T^{\mathrm{min}} = 6,8,11,15$ GeV as measured by ZEUS [27]. The solid curves correspond to requiring $E_T^{\mathrm{jet_1}}, E_T^{\mathrm{jet_2}} > E_T^{\mathrm{min}}$ while the dashed curves correspond to the cuts used in [12], as described in text.

KTCLUS algorithm used to define the jets. No systematic cut-off dependence was observed for these results, within the limitations of the Monte Carlo errors. The solid curves display the same trend that was observed in the single inclusive plots discussed previously insofar as the direct component comes closer to the data than does the resolved, the data are underestimated in the low E_T region, and the agreement gets better as E_T^{min} increases. This is consistent with there being some residual underlying event contribution to the observed jets which has not been removed during the data analysis.

The problem of defining a sample of two jet events in a manner which is amenable to a next-to-leading order theoretical treatment has been studied in [12]. In order to avoid a dependence on the theoretical cutoffs used in the course of the calculation, it was proposed to calculate the dijet cross section by allowing the second jet to have a transverse energy less than E_T^{min} if the third unobserved jet is soft, i.e., has a transverse energy of less than 1 GeV ($E_T^{\mathrm{jet_3}} < 1$ GeV). This approach slightly expands the available phase space when both jets have transverse energies near E_T^{min} and, therefore, avoids the problem of a potential cutoff dependence. Results using this algorithm are shown in Figs. 11 and 12 by the dashed lines. The relaxation of the E_T^{min} constraint on the second jet generates additional contributions from the $2 \to 3$ subprocesses so that the dashed curves lie above the solid ones and are in better agreement with the data. However, the cuts do not correspond to those utilized in the definition of the data sample. Given the unresolved question of the underlying event contributions, it is premature to draw detailed conclusions from comparisons with these data.

Angular distributions in dijet production are sensitive to the spin of the exchanged particle. Let θ^* be the scattering angle of the two highest E_T jets in their center of mass. In LO, the direct component is dominated by t-channel quark exchange which has a characteristic angular dependence given by $(1 - |\cos\theta^*|)^{-1}$. The resolved component, however, is dominated by t-channel gluon exchange and has a $(1$

$- |\cos\theta^*|)^{-2}$ angular dependence. This property is preserved at NLO as demonstrated by the solid lines in Fig. 13 where the dijet angular distribution $d\sigma/d|\cos\theta^*|$ is shown as a function of $|\cos\theta^*|$ in the regions $x_\gamma > 0.75$ (left) and $x_\gamma < 0.75$ (right) for the 1994 ZEUS conditions with $R = 1$, and $R_{\mathrm{sep}} = 2$. Also shown in the figure is the ZEUS [29] measurement and the LO (dash line) result. To better compare shapes, the distributions are normalized to one at $|\cos\theta^*| = 0$. The shapes are very insensitive to how one handles the dijet definition issue discussed above. The excellent agreement between the predictions and the data confirms the theoretically expected behavior.

IV. CONCLUSION

In this paper, results from a new next-to-leading order program for jet photoproduction have been presented. The calculation was performed using the phase space slicing method and implemented in a Monte Carlo style program. Physical observables are independent of the phase space slicing parameters.

As is the case in other jet production processes, the renormalization and factorization scale dependence is reduced relative to leading order predictions. A decomposition into direct and resolved components was also studied using a definition based on the observed momentum fraction of the parton from the photon. The direct component dominates at large E_T and in the photon direction while the resolved dominates at low E_T and in the proton direction.

Comparisons with single inclusive jet cross section measurements by H1 and ZEUS as a function of E_T^{jet} and η^{jet} show that the theory tends to lie somewhat below the data in the forward rapidity region. This is the region corresponding to low values for x_γ and which is dominated by the resolved component. One might suspect that this indicates a need for increasing the size of the photon parton distributions in this x range, but this conclusion would be premature since contri-
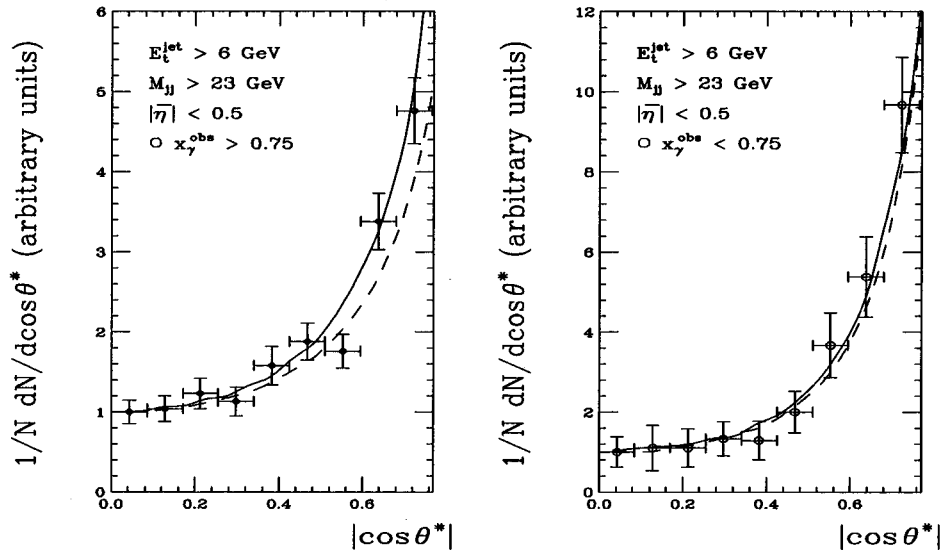
FIG. 13. Dijet angular distribution $d\sigma/d|\cos\theta^*|$ as measured by ZEUS [29] normalized to one at $\cos\theta^*=0$ compared with LO (dash lines) and NLO result (solid lines).

butions from underlying event structure could account for this, as well.

Our results were also compared with dijet cross section measurements from ZEUS. The cuts used to define the dijet sample are such as to restrict a portion of the phase space needed to ensure the proper cancellation of the cutoff dependence in the two- and three-body contributions. In practice, however, the variation was found to be smaller than the statistical errors associated with the Monte Carlo integrations. This point aside, the predictions for the normalized angular distributions agree well with the data. The $\bar{\eta}$ distributions show the same pattern of deviations from the theoretical predictions as was observed in the single inclusive jet measurements.

As additional data are acquired it is possible that jet photoproduction will be used to place additional constraints on the parton distributions in the photon. Such data would complement data for the photon structure function which are primarily sensitive to the quark distributions in the photon. The jet photoproduction process, on the other hand, directly involves the gluon distribution in the photon. However, in order for such data to provide useful constraints on the photon parton distributions, the effects of the underlying event structure must be minimized. Higher E_T thresholds combined with a smaller cone size in the jet definition would help in this regard.

[1] J. F. Owens, Phys. Rev. D **21**, 54 (1980).

[2] M. Drees and R. Godbole, J. Phys. G **21**, 1559 (1995).

[3] H. Baer, J. Ohnemus, and J. F. Owens, Phys. Rev. D **40**, 2844 (1989).

[4] D. Bödeker, Phys. Lett. B **292**, 164 (1992); Z. Phys. C **59**, 501 (1993).

[5] M. Klasen and G. Kramer, Z. Phys. C **72**, 107 (1996).

[6] L. E. Gordon and J. K. Storrow, Phys. Lett. B **291**, 320 (1992).

[7] M. Greco and A. Vicini, Nucl. Phys. **B415**, 386 (1994).

[8] P. Aurenche, J.-Ph. Guillet, and M. Fontannaz, Phys. Lett. B **338**, 98 (1994). The results for the resolved component in this paper are overestimated by a factor of 2, see [13].

[9] G. Kramer and S. G. Salesch, Z. Phys. C **61**, 277 (1994); D. Bödeker, G. Kramer, and S. G. Salesch, *ibid.* **63**, 471 (1994); M. Klasen, G. Kramer, and S. G. Salesch, *ibid.* **68**, 113 (1995).

[10] G. Kramer, J. Phys. G **22**, 717 (1996).

[11] B. W. Harris and J. F. Owens, in *Minneapolis Meeting of the Division of Particles and Fields of the American Physical So-ciety*, Minneapolis, 1996, edited by J. K. Nelson and K. Heller (World Scientific, Singapore, 1996), p. 453.

[12] M. Klasen and G. Kramer, DESY Report No. DESY 96-246.

[13] P. Aurenche, L. Bourhis, M. Fontannaz, and J.-Ph. Guillet, in *Proceedings of the Workshop 1995/96 on Future Physics at HERA*, Hamburg, 1996, edited by G. Ingelman *et al.* (Deutches Elektronen-Synchrotron, Hamburg, 1996), p. 570.

[14] L. J. Bergmann, Ph.D. thesis, Florida State University, 1989.

[15] C. F. Weizsäcker, Z. Phys. **88**, 612 (1934); E. J. Williams, Phys. Rev. **45**, 729 (1934).

[16] S. Frixione, M. L. Mangano, P. Nason, and G. Ridolfi, Phys. Lett. B **319**, 339 (1993).

[17] R. K. Ellis and J. C. Sexton, Nucl. Phys. **B269**, 445 (1986).

[18] P. Aurenche, R. Baier, A. Douiri, M. Fontannaz, and D. Schiff, Nucl. Phys. **B286**, 553 (1987). The expressions for the $qq\to qq\gamma$ and $qq'\to qq'\gamma$ subprocesses contain a number of typographical errors where the variable a_3 appears in place of a_5. The original report LPTHE Orsay 86/24 contains the correct expressions.

[19] J. Huth *et al.*, in *Proceedings of the 1990 DPF Summer Study on High Energy Physics*, Snowmass, Colorado, edited by E. L. Berger (World Scientific, Singapore, 1992), p. 134.

[20] S. D. Ellis, Z. Kunszt, and D. E. Soper, Phys. Rev. D **40**, 2188 (1989).

[21] H. L. Lai *et al.*, Phys. Rev. D **55**, 1280 (1997).

[22] M. Glück, E. Reya, and A. Vogt, Phys. Rev. D **46**, 1973 (1992).

[23] L. E. Gordon and J. K. Storrow, Nucl. Phys. **B489**, 405 (1997).

[24] ZEUS Collaboration, M. Derrick *et al.*, Phys. Lett. B **348**, 665 (1995).

[25] H1 Collaboration, S. Aid *et al.*, Z. Phys. C **70**, 17 (1996).

[26] ZEUS Collaboration, M. Derrick *et al.*, Phys. Lett. B **342**, 417 (1995).

[27] Y. Yamazaki, for the ZEUS Collaboration, in *Proceedings of the 28th International Conference on High Energy Physics*, Warsaw, 1996, edited by Z. Ajduk and A. K. Wroblewski (World Scientific, Singapore, 1996), p. 809.

[28] J. M. Butterworth, L. Feld, M. Klasen, and G. Kramer, in *Proceedings of the Workshop 1995/96 on Future Physics at HERA*, Hamburg, 1996, edited by G. Ingelman *et al.* (Deutches Elektronen-Synchrotron, Hamburg, 1996), p. 554.

[29] ZEUS Collaboration, M. Derrick *et al.*, Phys. Lett. B **384**, 401 (1996).